

Article

Seismostratigraphic Interpretation of Upper Cretaceous Reservoir from the Carpathian Foreland, Southern Poland

Andrzej Urbaniec ^{1,*}, Anna Łaba-Biel ¹, Anna Kwietniak ² and Imoleayo Fashagba ²¹ Oil and Gas Institute–National Research Institute, 25A Lubicz Str., 31-503 Kraków, Poland; laba-biel@inig.pl² Faculty of Geology, Geophysics and Environmental Protection, University of Science and Technology AGH, 30 Mickiewicz Av., 30-059 Kraków, Poland; anna.kwietniak@agh.edu.pl (A.K.); imolefashagba@gmail.com (I.F.)

* Correspondence: urbaniec@inig.pl

Abstract: The Upper Cretaceous complex in the central part of the Carpathian Foreland (southern Poland) is relatively poorly recognized and described. Its formations can be classified as unconventional reservoir due to poor reservoir properties as well as a low recovery factor. The main aim of the article is to expand knowledge with conclusions resulting from the analysis of the latest seismic data with the application of seismic sequence stratigraphy. Moreover, the seismic attributes analysis was utilized. The depositional architecture recognition based on both chronostratigraphic horizons and Wheeler diagram interpretations was of paramount importance. A further result was the possibility of using the chronostratigraphic image for tectonostratigraphic interpretation. Two distinguished tectonostratigraphic units corresponding to megasequences were recognized. A tectonic setting of the analyzed interval is associated with global processes noticed by other authors in other parts of the central European Late Cretaceous basin, but also locally accompanied by evidence of small-scale tectonics. This study fills the gap on the issue of paleogeography in the Late Cretaceous sedimentary basin of the Carpathian Foreland. It presents the first results of detailed reconstruction of the basin paleogeography and an attempt to determine the impact of both eustatic and tectonic factors on sedimentation processes.

Keywords: Upper Cretaceous; seismic sequence stratigraphy; seismic attributes; Wheeler diagram



Citation: Urbaniec, A.; Łaba-Biel, A.; Kwietniak, A.; Fashagba, I.

Seismostratigraphic Interpretation of Upper Cretaceous Reservoir from the Carpathian Foreland, Southern Poland. *Energies* **2021**, *14*, 7776. <https://doi.org/10.3390/en14227776>

Academic Editor: Reza Rezaee

Received: 18 October 2021

Accepted: 17 November 2021

Published: 19 November 2021

Publisher's Note: MDPI stays neutral with regard to jurisdictional claims in published maps and institutional affiliations.



Copyright: © 2021 by the authors. Licensee MDPI, Basel, Switzerland. This article is an open access article distributed under the terms and conditions of the Creative Commons Attribution (CC BY) license (<https://creativecommons.org/licenses/by/4.0/>).

1. Introduction

Mesozoic carbonate formations are the subject of research in many regions of the world because they are a good collector for the accumulation of oil and gas [1–10]. In the area of the central part of the Carpathian Foreland, the carbonate complex of the Upper Jurassic and Lower Cretaceous sediments is relatively well recognized [11–18]. The maximum thickness of this complex is approximately 1300 m [12,18]. In contrast, the carbonate-clastic Upper Cretaceous deposits, although they lie much shallower and have been drilled by numerous wells, are much less recognized. Their maximum thickness in the study area is 400 m (Figure 1; Supplementary Materials Figure S1). Knowledge regarding the mechanisms of sedimentation of these formations, directions of transport, and paleogeography of the sedimentary basin during the Late Cretaceous is still scarce. Therefore, the main aim of our article is to expand the knowledge with conclusions resulting from the analysis of recent seismic 3D data located in the central part of the Carpathian Foreland. The newly acquired, high-resolution seismic data allow for multiple analyses, previously not possible to be applied in this area. This contributes to a much better understanding of the architecture of a difficult to interpret marginal part of the Late Cretaceous sedimentary basin of central Europe. Furthermore, our research can fill the gap between insight from core analysis and seismic data interpretation.

The Upper Cretaceous formations are better studied in the areas adjacent to the Carpathian Foreland, i.e., Miechów Trough and the vicinity of Kraków city, where the Upper Cretaceous rocks are exposed on the surface [19–24]. Only a small number of

publications are devoted exclusively to the Upper Cretaceous deposits of the central part of the Carpathian Foreland, despite the relatively good documentation of the spatial extent and stratigraphic column of these deposits in the wells. Most attention in publications was devoted to the Cenomanian interval composed of siliciclastic rocks [25–27], mainly due to the discovery of several commercial oil and gas accumulations. However, in our area of study the Cenomanian sediments are absent or their thickness is very small, about several meters.

The most comprehensive work describing the entire succession of the Upper Cretaceous deposits from the central part of the Carpathian Foreland was published by Heller and Moryc in 1984 [28]. This work is the only one containing full lithological description of the Upper Cretaceous succession, records of observed erosion surfaces, and characteristic assemblages of foraminiferal microfauna for Upper Cretaceous stages. All information was compiled strictly on the basis of well data. The mentioned work contains significant and detailed biostratigraphic conclusions as well as rough suggestions concerning tectonic development of the area.

There are no published works on Upper Cretaceous formations from the study area based on interpretation of seismic data.

The interest in the mixed carbonate-clastic formation is related to the discovery of several hydrocarbon deposits in the Turonian–Maastrichtian complex in the second half of the 1980s [29,30]. However, variable and mostly poor reservoir properties as well as low oil recovery factors make this carbonate-clastic reservoir be classified as unconventional. The difficulty to predict lithological variability of these deposits is a great obstacle in interpretation, as well as their relatively poor identification on 2D seismic sections, which significantly increases the exploration risk. As a result, there were no further discoveries of oil and gas fields in the research area. The high-quality 3D seismic survey performed in recent years has provided new possibilities for the analysis of the Upper Cretaceous formations. Based on seismic data, it was possible to apply seismic attributes and spectral decomposition, which are considered basic tools in seismic interpretation [31–36]. Novel approach in interpretation applied for this region was based on both chronostratigraphic image and Wheeler diagram interpretation. Together with thorough sequence stratigraphy method application, it was possible to understand complex processes, not only connected with depositional architecture, but also with the tectonic framework. Such an approach provides insight into understanding the depositional history as well as the paleomorphology of the studied Late Cretaceous subbasin.

Older publications [37–40] contain only general and very scarce descriptions of the Upper Cretaceous formations, composed within the framework of characterizing the entire lithostratigraphic profile of the Carpathian Foreland. In more recent works, partly dealing with the subject of the Upper Cretaceous sediments, slightly more complete descriptions and generalized interpretations of these formations have been presented, such as in the works of Machaniec and Zapałowicz-Bilan or Moryc [41,42].

This study fills the gap on paleogeography topic in the Late Cretaceous sedimentary basin of the Carpathian Foreland situated on the southwestern edge of the East European Craton. Authors present a unique study combining seismostratigraphic analysis and seismic attributes interpretation, that enabled, for the first time, to reconstruct the paleoenvironmental relations. It should be noted that until now, there were no works that addressed this issue due to the lack of sufficient data quality and the very complicated nature of the Upper Cretaceous succession resulting from both sedimentary and tectonic factors.

2. Geological Setting

The study area is located in southern Poland within the central part of the Carpathian Foreland area (Figure 1).

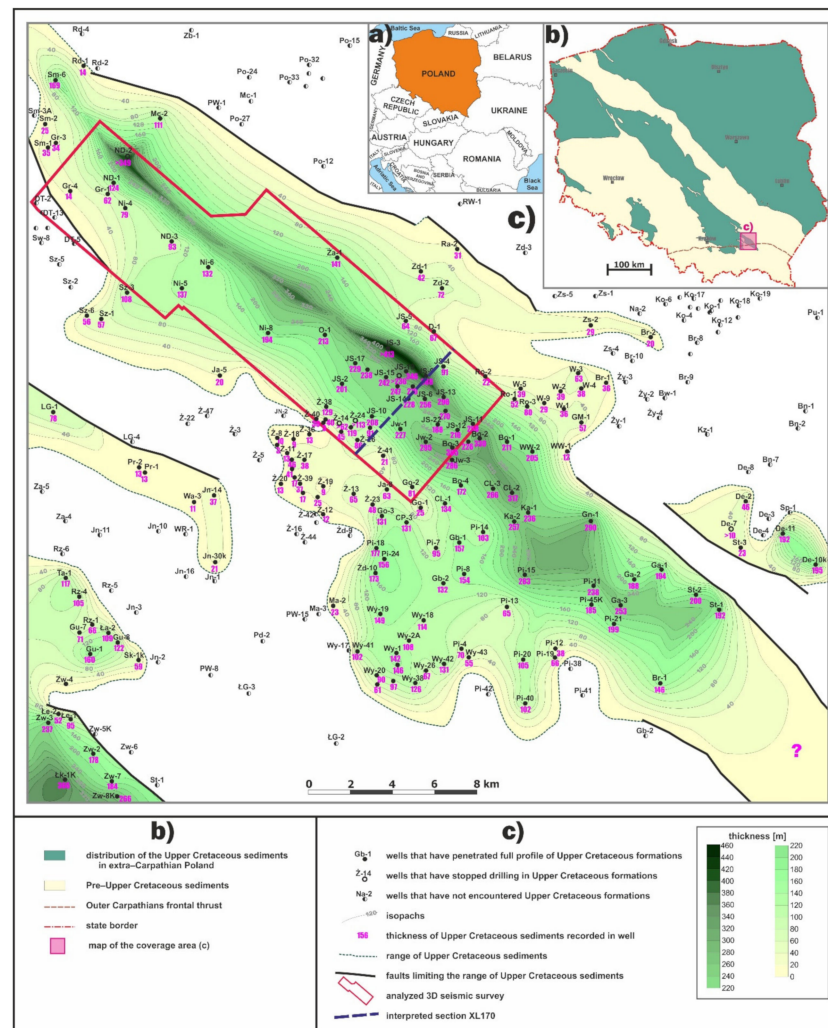


Figure 1. Location of the study area: (a) generalized outline of central Europe; (b) location of the study area (pink rectangle) in relation to the distribution of the Upper Cretaceous formations in extra-Carpathian Poland (modified after Walaszczyk et al., 1999 [43]); (c) isopach map of the Upper Cretaceous formations in the study area.

The oldest structural stage in the research area is represented by a series of Neoproterozoic anchimetamorphic rocks. The Ediacaran age of that complex is confirmed by the results of micropaleontological analyses carried out on samples from the wells [44,45]. The middle stage is composed of Meso-Paleozoic rocks of a considerable summary thickness up to 2000 m. The Ordovician and Silurian full deposits are situated in the southern part of the analyzed region, directly on the Ediacaran interval. Higher up in the section lie the carbonate series of Devonian and Carboniferous sediments [46,47]. The Mesozoic interval is represented by carbonate and clastic Triassic sediments, and above them lie mainly carbonate Jurassic and Cretaceous complexes [12,15,48]. The youngest structural stage is formed by the Miocene formations (Badenian–Sarmatian), which were initially deposited in the Carpathian Foredeep basin. The complex of autochthonous Miocene strata in the research area can be divided into three main units: the Lower Badenian clastic sub-evaporite series, the Upper Badenian evaporate series, and the Upper Badenian–Sarmatian clastic series [49,50].

The Upper Cretaceous formations were deposited above the regional unconformity observed above the Lower Cretaceous or Upper Jurassic formations. The structural position of these formations in the first stages of sedimentation distinctly reflects the paleomorphology of the older substrate. Their range and thickness in the Carpathian Foreland are very

diverse (Figure 1; Supplementary Materials Figure S1). This is the result of tectonic and erosive processes that took place during the Late Cretaceous, Palaeogene, and Neogene periods. The primary differences in thickness of the Upper Cretaceous formation may be result of the differentiation of sedimentation and subsidence rate of the sedimentary basin [13,51]. However, the greatest thickness variation is the consequence of post-Laramian erosion resulting in complete removal of the Upper Cretaceous sediments from the part of the area (Figure 1; Supplementary Materials Figure S1).

In general, the Upper Cretaceous section in the area of the Carpathian Foreland can be divided into two main complexes: the lower clastic complex, which includes Cenomanian sediments, and the upper mixed carbonate-clastic complex, composed of Turonian–Maastrichtian sediments (Figure 2). The Cenomanian/Turonian transition is discontinuous. An anoxic event took place in the basin at that time, which was related to the rapid extinction of some benthic foraminifera [52,53]. The lower complex in the research area is only partially developed, and its thickness does not exceed 15 m (thus below the seismic resolution). The thickness of the upper complex in the study area is very differentiated, ranging from 0 to approximately 460 m (Figure 1; Supplementary Materials Figure S1). Within the upper complex in the area of the Carpathian Foreland, all stratigraphic stages (from Turonian to Maastrichtian) were micropalaeontologically dated, while in the wells located directly in the study area, the stages from Turonian to Campanian were dated [28,42].

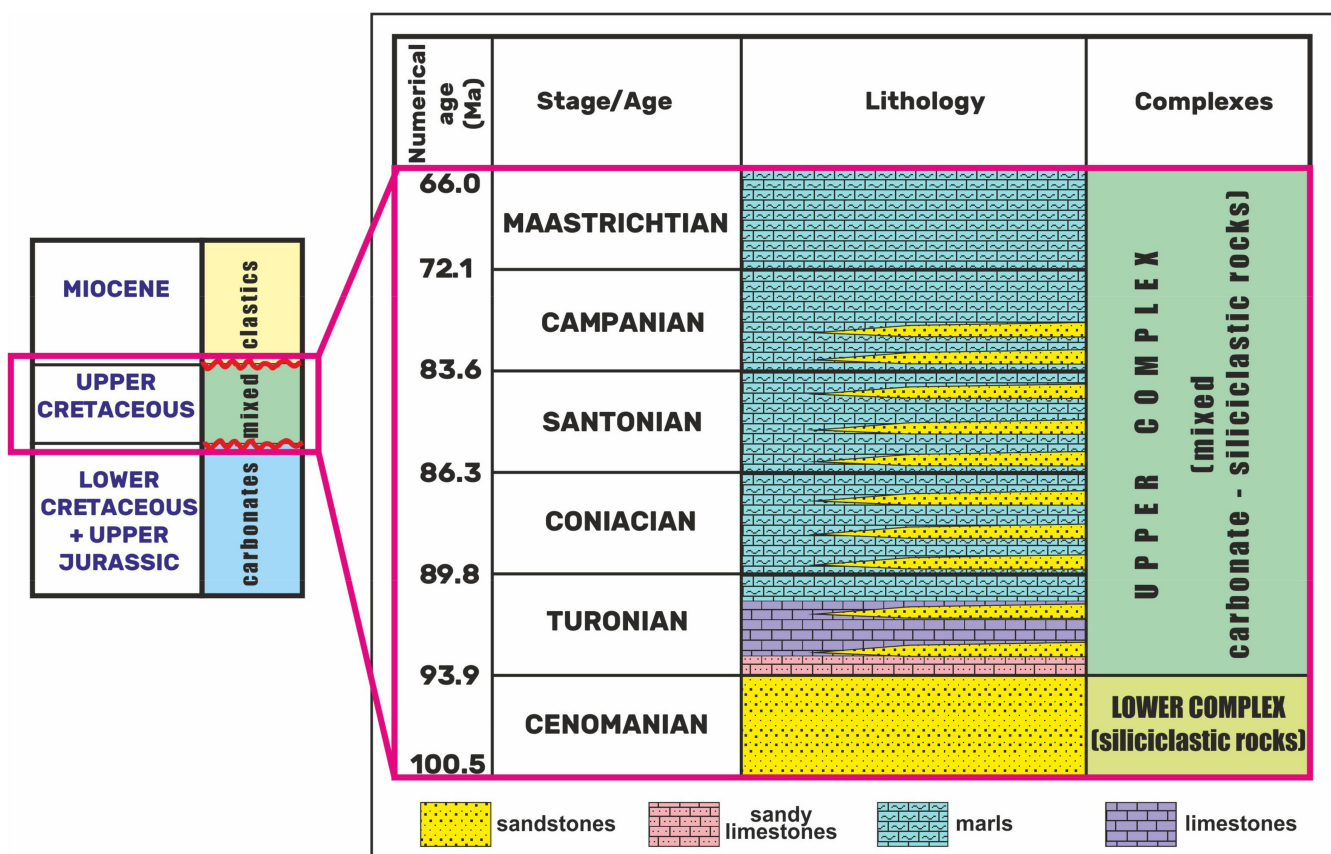


Figure 2. Generalized lithological scheme of the Upper Cretaceous formation in the area of the central part of the Carpathian Foreland.

3. Materials and Methods

3.1. Data Description

The seismic data used for the project are 3D seismic data that were acquired in 2015. The survey covered an area of about 150 km² (bin size 20 × 20 m) and was obtained by both dynamite and vibroseis methods. The data were processed with a relative ampli-

tude preservation scheme, and the resulting volume is a migrated seismic section in the time domain with a sampling rate of 2 ms. The volume was calibrated to the geological information with the use of 15 wells with sonic logs that exist within the survey area.

3.2. Seismic Sequence Stratigraphy

Seismic stratigraphic analysis of the chronostratigraphic image and the Wheeler diagram are the main interpretative tools for understanding and reliable reconstruction of the depositional architecture. For this purpose, the entire 3D seismic cube is postprocessed by using the procedure of layer-dip identification. With the information of dip direction and angle a semi-automatic procedure that indicates directivity of seismic horizons is applied. The resulting image reveals chronostratigraphic events on seismic profile.

Accurate selection of seismic lines from 3D images is an important stage of research. The azimuth of the selected lines should be consistent with the general direction of deposition of the analyzed formations and reflects the geometrical relationships occurring in the sedimentary basin. Chronostratigraphic image and Wheeler diagram are constructed for the selected seismic lines and hence provide detailed information about the deposition applicable for the chosen azimuth.

Seismic sections with chronostratigraphic horizons that enable the reconstruction of the depositional history are calculated in the time gate defined by selected seismic horizons, which most often correspond to the stratigraphic boundaries [54,55]. In principle, the gate should cover a greater time range, and not only refer to the interval of focus. Such a procedure allows to avoid interpretation errors during correlation, especially in areas not recognized by drilling.

With the set of the chronostratigraphic horizons, it is possible to construct a Wheeler diagram. The transformation to the Wheeler domain requires flattening of the chronostratigraphic horizons and assigning them to a relative geological time scale [54,56]. A Wheeler diagram is calculated to identify and visualize a lateral range of sedimentary episodes, hiatuses (erosive events or periods without deposition), and deposition directions [56,57].

3.3. Tectonostratigraphy

Tracking the continuity of the chronostratigraphic horizons is essential for the recognition of the tectonic history of the sedimentary basin area [58,59]. The interruption of the continuity of the chronostratigraphic horizons may indicate various phenomena such as lack of sedimentation, erosion, or tectonic processes [60,61]. The integration of the sequence stratigraphy methodology with fault interpretation made it possible to distinguish structural units characterized by a different tectonic style corresponding to megasequences. The term “megasequence” is understood as tectonostratigraphic complex of sediments deposited during the crucial phases of the sedimentary basin development [60,62,63]. Tectonostratigraphic units can correspond to regional events such as contractional and extensional phases of basin development [59,64,65]. Sound knowledge of the geology of a given region, combined with a detailed interpretation of the depositional sequences, allows to correctly define the mechanisms influencing the current structural image of the analyzed formation.

3.4. Seismic Attributes and Spectral Decomposition

Seismic attributes that are the most helpful for depositional architecture recognition are envelope, root mean square (RMS) amplitude, and sweetness. Additionally, spectral decomposition based on fast Fourier transform (FFT) was also performed.

3.4.1. Envelope, RMS Amplitude, Sweetness

Seismic attributes used for this study are based on the amplitude and frequency values. These attributes are efficiently computed and have been used to gain insight into seismic image for several decades [31,32,35,36,66–69]. The simplicity of the algorithms, that are

mostly based on the Hilbert transform and basic statistics [70], makes them straightforward for application and effective.

Many attributes were applied and tested in research, such as coherence attribute, ant tracking, instantaneous frequency, and phase. Similarly, for spectral decomposition, the CWT algorithm was run as well. The presented set of attributes and spectral decomposition depicts the best depositional architecture. Authors decided to show only those results that yielded new insight into the interpretation.

Envelope presents the total instantaneous energy of the complex trace, which is independent of phase. It is also known as instantaneous amplitude or reflection strength [70,71]. For visualization of the attribute value on the map a window length of 33 ms was used, in which the value of attribute was averaged and assigned to the surface of interests.

RMS amplitude is the square root of the sum of the squared amplitudes [70], divided by the number of samples. In the computations, a window of 9 samples (that equals to 18 ms) was used. RMS amplitude is helpful in the identification of hydrocarbon concentrations. It is useful for the interpretation of depositional environments [31,72], by exhibiting different amplitude responses (different value of attribute as well as gradient of changes).

Sweetness is a combination of instantaneous amplitude and instantaneous frequency. It is particularly helpful to indicate the overall energy changes within the seismic data that can be linked to lithological changes [73–75]. The sweetness attribute is useful for paleoenvironmental characteristics and depositional architecture identification.

For all the applied attributes, different color scales were implemented, the scale was adjusted to the extreme values, and specific color pallets were tested. It was noted that a simple technique of changing a color palette enabled more detailed interpretation.

3.4.2. Spectral Decomposition

The spectral decomposition process enables to assign amplitude values to different frequency components. The process can be understood as multi-dimensional frequency filtering that results with frequency volumes that show reflection's amplitude specific to this spectral component. Spectral decomposition can be used for thin bed thickness identification [76], tuning analysis [27], and hydrocarbon identification [77]. Different algorithms have been proposed for the computational process; among the most popular are fast Fourier transform (FFT) [78], continuous wavelet transform (CWT) [77], matched-pursuit decomposition (MPD) [79], and complete ensemble empirical mode decomposition (CEEMD) [80].

Spectral decomposition may be also used for depositional architecture interpretation and allows to image elements such as channels, fans, confined channel axis, wedges, deltaic systems, clinoforms, etc. Spectral decomposition was previously used for such purposes within the area of interest, especially for the Miocene [75,81–83].

Two algorithms of spectral decomposition were utilized in this study; results differ in terms of image quality and resolution. The results of spectral decomposition presented in this paper are based on the FFT method, which is considered to yield better results. The frequencies applied were chosen based on a visual inspection of the amplitude spectrum of the seismic data. The most useful frequencies for the spectral decomposition were found to be 19 Hz, 24 Hz, and 35 Hz. These frequencies were blended [31] using the CMYK (cyan, magenta, yellow, key-black) color scale.

4. Results

The analyzed Upper Cretaceous formations representing facies dominated by carbonate sediments with a minor admixture of siliciclastics are very difficult to interpretation. This is mainly due to the small thicknesses of individual depositional sequences (below the seismic resolution), subtle horizontal and vertical facies diversity, variability of the directions of sedimentary material supply to the sedimentary basin, and high tectonic involvement. For these reasons, the standard methods of interpretation used so far did not

allow for the identification and reconstruction of the depositional architecture of the Upper Cretaceous basin in the study area.

The chronostratigraphic image and the Wheeler diagram were calculated for two seismic lines with the SW-NE azimuth. Results of the interpretation are presented only for the XL170 section (location in the Figure 1c; Supplementary Materials Figure S1). The research covered the time interval determined by the Intra-Jurassic seismic horizon and the boundary associated with the Miocene evaporative series (Ma). The colors of the obtained chronostratigraphic horizons are linked to the relative geological ages of the events [54] (Figure 3b).

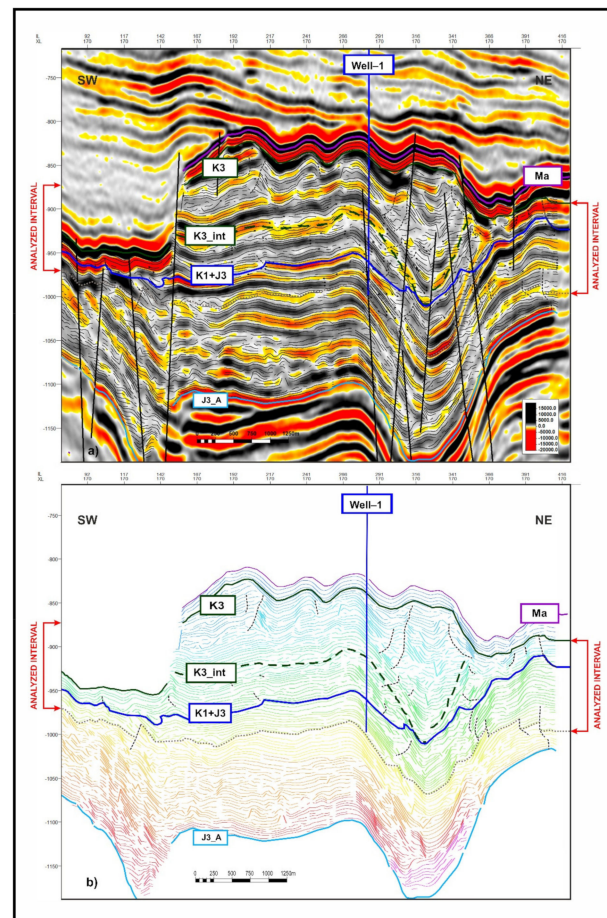


Figure 3. Main seismic horizons shown against chronostratigraphic horizons calculated by the data-driven approach: (a) chronostratigraphic horizons shown at the background of the time seismic section; (b) chronostratigraphic horizons in the color scale.

The performed interpretation of the chronostratigraphic horizons and the Wheeler diagram for the Upper Cretaceous deposits was based on the assumptions of the sequence stratigraphy methodology [84–87] as well as the carbonate and mixed carbonate-siliciclastic sedimentary basins depositional models [85,88–90].

It should be noted that there exists an ongoing discussion on a methodology for sequence boundaries interpretation and the specialistic nomenclature [85–87,91,92]. Nonetheless, in the presented material, we decided to divide sequence boundaries into two types: type I and type II [93], even though recently type II discontinuities have been considered to be an integral part of the failing stage systems tracks (FSST; shift of the shore-line basinward during one sequence with the fall of relative sea level).

In the entire interpreted interval, the analysis of the configuration, continuity, and contacts of the simultaneous horizons was performed. The chronostratigraphic horizons in the Wheeler diagram show a hierarchical alignment, and their arrangement interpreted in

the direction of deposition allows to define individual sequences of depositional system. However, only the simultaneous interpretation of the chronostratigraphic volume and the Wheeler diagram allow to determine the depositional sequences. In total, 31 depositional sequences were identified and traced, 23 of which are located within the Upper Cretaceous section (Figure 4; Supplementary Materials Figure S2). Most of the interpreted depositional sequences have well-defined sequence boundaries. Thanks to this, it was possible to determine and trace the sequence boundaries (SB) and the maximum flood levels (mfs).

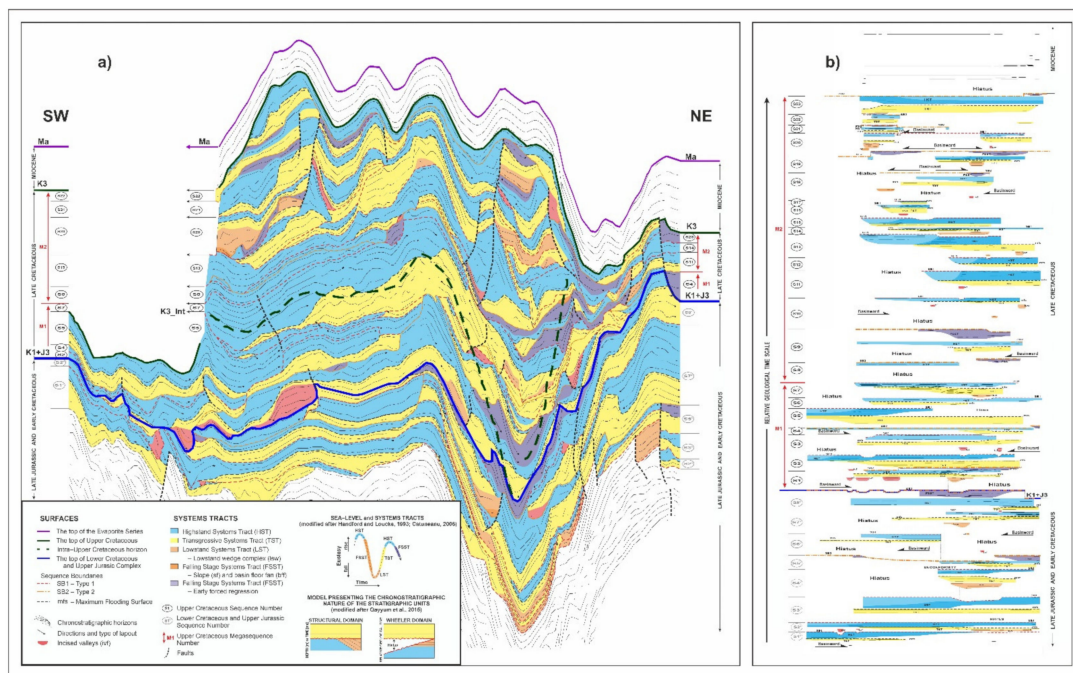


Figure 4. Detailed sequence stratigraphy and tectonostratigraphy interpretation of (a) chronostratigraphic horizons in structural domain and (b) Wheeler diagram transformed from seismic data.

The chronostratigraphic image allowed to distinguish two types of depositional sequences and related sequence boundaries (SB1 and SB2). The differences between the depositional sequences focus on the individual nature of the falling stage systems tracks (FSST). The depositional sequences associated with the erosive boundary of SB1 and its correlative accordance were deposited in conditions of a relatively rapid sea-level fall. The configuration of chronostratigraphic horizons and the geometry of the type I sequence boundary allow the identification of the depositional elements typical for deposits, such as incised valleys, slope fans, and basin fans. Depositional sequences associated with the boundary of type II are generally characterized by a deposition of FSST sediments of an aggradational nature in the shelf edge zone. Sequences of this type are characterized by a steep morphology of the slope zone. The material from the destroyed edges of the shelf is deposited in the form of submarine landslides and debris flows.

The determined sequence boundaries were differentiated by using different colors. Type I (SB1) boundaries are shown in red and type II (SB2) boundaries are shown in orange (Figure 4; Supplementary Materials Figure S2).

With such an approach, it was possible to identify typical elements of the depositional architecture for carbonate and mixed carbonate-siliciclastic sedimentary basins, genetically related to the systems tracts of the depositional systems (LST, FSST, TST, and HST) [54,85–88]. Such elements include, for example, barriers, incised valleys, or packages of deposits created as a result of gravity flows.

As a result, the depositional history of the analyzed sedimentary complexes was reconstructed. In the presented section, several stratigraphic gaps of different natures and local or regional character are indicated. Based on a comprehensive interpretation

of the chronostratigraphic image, time-varying transport directions were determined (Figure 4b—marked with arrows; Supplementary Materials Figure S2). Moreover, it was possible to interpret various elements of the paleoenvironment, with the determination of their mutual spatial relations.

In the chronostratigraphic image, discontinuity surfaces are visible, which can be interpreted as small-scale, local faults (Figure 4a, dashed black lines; Supplementary Materials Figure S2). It is worth noting that most of these dislocations are not visible in the seismic image (compare Figures 3 and 4a).

The integration of the sequence stratigraphy methodology with fault interpretation made it possible to distinguish two structural complexes characterized by a different tectonic style within the Upper Cretaceous interval, corresponding to megasequences. Each of the distinguished tectonic sequences is characterized by a different chronostratigraphic image, a specific layout of horizons in the Wheeler diagram, and a specific system of faults. Each of the distinguished megasequences is closely related to the different stage of the geological history of a investigated region [65]. The megasequence tops are determined by erosive and angular discrepancies or a combination of seismic reflection contacts: downlap and onlap [60].

The analyzed segment of the Upper Cretaceous basin of the Carpathian Foreland can be understood as a specific subbasin, which borders are controlled by faults. The development of this type of basin involves a number of different stages closely related to the contractional and extensional phases [65,94]. These phases are accompanied by such phenomena as the changes in the sea level, episodes of intensive erosion that may lead to the peneplanation of the adjacent land area, and tectonic quiescence [95,96].

The interpreted Upper Cretaceous depositional sequences in the study area were divided into two main megasequences: lower (M1) and upper (M2) (Figure 4; Supplementary Materials Figure S2), characterized by a diverse structure. A stratigraphic hiatus was identified between these megasequences.

The lower megasequence (M1) is built by seven depositional sequences S1–S7 (Figure 4; Supplementary Materials Figure S2) covering almost the entire area of the analyzed segment of the sedimentary basin. Each of these sequences is characterized by a complete structure of the depositional systems tracts. Moreover, there are no major tectonic disturbances in the entire profile of the lower megasequence (M1). These features indicate that at this stage of development, the Upper Cretaceous sedimentary basin was in a tectonic quiescence and subordinate faults were probably the result of stress relaxation and differential loading.

Much greater influence of tectonic processes is noticeable in the construction of the upper megasequence (M2), separated from the lower with the above-mentioned sedimentary hiatus and represented by the depositional sequences S8–S23 (Figure 4, Supplementary Materials Figure S2). The system of chronostratigraphic horizons indicates that the analyzed area underwent a significant shortening, which was initially related to the uplift and rotation of individual tectonic blocks. The shortening stage was particularly well recorded in the central, depressed part of the sedimentary basin, within which a small-scale tectonic squeezing and tilting of the older Upper Cretaceous deposits (building the lower megasequence) took place, leading to a noticeable increase in their apparent thickness. Such basin geometry suggests that the analyzed area most likely underwent compression reactivation, which is consistent with the theory that during the Late Cretaceous, there was a global period of basin inversion tectonic [13,97–103]. In the higher part of the upper megasequence in the chronostratigraphic image, it is also possible to interpret the effects of the process of walls collapsing along large normal faults limiting the tectonic depression zone. Such structures may indicate the extensive nature of the sedimentary basin [94,104,105].

In order to confront the results of the high-resolution interpretation method with the conventional structural seismic interpretation, a local correlation of the Intra-Upper Cretaceous (K3_int) seismic horizon was performed in the seismic image (Figures 3 and 4a). This horizon was correlated in the lower, less tectonically disturbed part of the Upper

Cretaceous profile. It is associated with the most visible and continuous positive seismic reflection. The comparison of the interpreted K3_int seismic horizon against the background of the seismostratigraphic interpretation based on the chronostratigraphic image showed that this horizon is not closely related to any of the interpreted depositional sequences. The correlated K3_int horizon intersects the deposit sequences at different positions of the chronostratigraphic column.

Based on the interpreted seismic horizon K3_int, maps of surface seismic attributes were calculated (spectral decomposition—Figure 5a, sweetness—Figure 5b, RMS amplitude—Figure 5c, envelope—Figure 5d). It was possible to trace the development and spatial extent of various elements of depositional architecture on the attribute maps. As the K3_int horizon crosses different depositional sequences (Figure 4a; Supplementary Materials Figure S2), it should be emphasized that the elements of the depositional architecture interpreted in the maps belong to different systems tracts. The combination of the interpretation of the attribute maps with the results of the chronostratigraphic interpretation allowed for a better understanding of their geometric and genetic relationships.

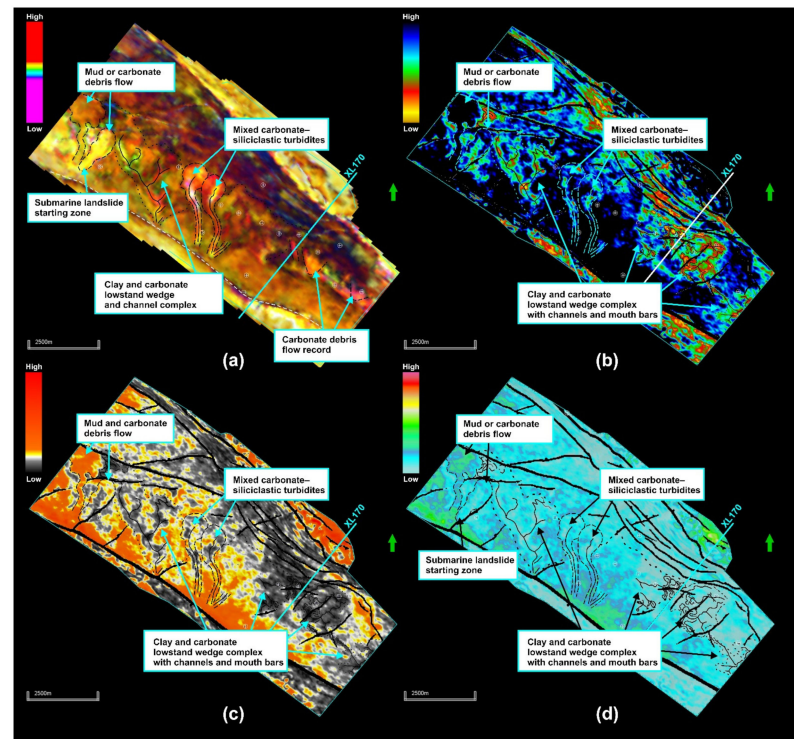


Figure 5. Maps presenting depositional architecture elements interpreted with the results of spectral decomposition and seismic attributes shown at K3_int surface: (a) spectral decomposition based on FFT algorithm; (b) sweetness; (c) RMS amplitude; and (d) envelope.

Comprehensive analysis of all the aforementioned attribute maps allowed to identify the anomalous zones related to the specific elements of the depositional architecture. The sweetness attribute and spectral decomposition were considered the most helpful in interpretation. The elements of the depositional architecture identified on these maps, characterized by a large diversity of geometry, can be associated with the deposition in various phases of sea level fluctuations (Figure 5).

Based on the shapes of anomalous zones in attribute maps (Figure 5a–d), the following elements of depositional architecture were identified: barriers, distribution channels and channelized lobes formed in the conditions of rising sea level (TST), and debris flows, which can be associated with both high sea level (HST) and low sea level (LST). Additionally, submarine landslide starting zones can be recognized in the maps of spectral decomposition (Figure 5a) and envelope (Figure 5d). They are characterized by a specific oval-shaped

contour. Lowstand wedge complex associated with the distribution channels is another element of the depositional architecture interpreted based on spectral decomposition (Figure 5a) and the sweetness attribute (Figure 5b). The existence of these types of deltas may suggest an increase in the proportion of siliciclastic material in the sedimentary basin [85,87,88]. The sweetness attribute map provided the best insight into the basin morphology, revealing precisely the distribution of channels associated with mouth bars. It has been observed that in many places these channels run along the interpreted fault planes (Figure 5b).

5. Discussion

The complicated mixed carbonate-clastic Upper Cretaceous sedimentary complex developed on the southwestern edge of the East European Craton is still characterized by poor geological recognition. Such issues as the mechanisms of sedimentation, the directions of transport, and the paleogeography of the sedimentary basin are still under discussion [13,51,102,106–108]. An essential question is to estimate the impact of tectonic processes on the development of the sedimentary basin and changes of its geometry during the Late Cretaceous period [100,102,103,109,110].

The specific character of studied mixed carbonate-clastic reservoir that manifests mostly poor reservoir properties and low recovery factor requires an unconventional and more detailed approach in the interpretation of seismic data. Interpretation beginning with a detailed analysis of seismic data allows for a better understanding of the paleogeographic relationships in the sedimentary basin and consequently to lithofacial diversity of the studied formations. This type of interpretative approach can lead to more precise identification of prospects in both conventional and unconventional exploration.

According to the study, the depositional sequences associated with individual sedimentary episodes are characterized by small thicknesses, often below the resolution of the seismic data. Therefore, the interpretation of seismic data conducted so far did not allow to reliably reconstruct too many details of depositional architecture within the sedimentary basin. It should be concluded that due to the high facies variability and small thicknesses of individual depositional sequences, the conventional seismic interpretation is not suitable for reconstruction of the depositional architecture of the Upper Cretaceous deposits. The methodology proposed in this paper, based on the seismic stratigraphic analysis of the chronostratigraphic image and the Wheeler diagram, provides the possibilities of a more detailed reconstruction of the sedimentary basin configuration including elements of the paleoenvironment. Furthermore, based on the chronostratigraphic image interpretation, it is possible to determine the main directions of sedimentary material supply to the Late Cretaceous sedimentary basin. Small-scale, local dislocations, in some cases not visible in the seismic image, can be revealed based on the discussed method. Using the entire collection of information obtained from the interpretation of the chronostratigraphic image, it is possible to reconstruct the full depositional and tectonic history of the analyzed segment of the Upper Cretaceous Foreland basin.

Interpreting and evaluating the structural map of K3_int horizon with the overlaid results of seismic attributes and spectral decomposition helped authors to understand that the horizon intersects various sedimentary episodes. With this observation, it was decided to perform chronostratigraphic analyses. Only after that was it possible to understand the complex nature of image seen on attributes maps. Such an approach revealed that the previously interpreted horizon, guided by picks from the wells and seismic image, was not stratigraphically consistent. Nonetheless, each attribute enabled to see different elements of depositional architecture. Currently, the authors are continuing analyses which are mostly directed towards editing K3_int horizon according to the chronostratigraphic image. So far, the preliminary result is that Upper Cretaceous deposits in the analyzed region are hugely diverse and tectonically involved.

The tectonic setting of the analyzed interval is associated with global processes observed in the Late Cretaceous basin, but also, locally accompanied by evidence of

small-scale tectonics. The application of the chronostratigraphic image computed by a data-guided approach enables to indicate discontinuities. The authors believe that this is partially due to the fact that computation of chronostratigraphic horizons is guided, among other things, by the dip of seismic reflections. Hence, it is highly recommended to test the chronostratigraphic image not only for seismic sequence stratigraphy analysis, but also for structural interpretation.

Performed studies provided an opportunity to identify numerous unconformities and hiatuses connected with erosive events or periods without deposition. The presence of numerous unconformities was described before by Heller and Moryc [28] based on the study of cores from this area. Moreover, a regional stratigraphic gap from the Late Coniacian to Early Santonian was identified in outcrops located within the neighboring Kraków area [107,111].

One of the major stratigraphic hiatuses was identified in between the two distinguished tectonostratigraphic units corresponding to megasequences. The lower one (M1) is built by several depositional sequences, characterized by a complete structure of the depositional systems tracts. No major tectonic disturbances have been detected in this part of section representing the layer-cake depositional model. Much greater influence of tectonic processes is noticeable in the structure of the upper megasequence (M2). This part of the Upper Cretaceous sequence is much more complicated as a result of the uplift and rotation of individual tectonic blocks, as well as the effect of the next phase of the extensive basin inversion. A very similar type of bi-partite structure of the Upper Cretaceous section was recently described by Stachowska and Krzywiec [102] from the Grudziądz–Polik area situated in central Poland. The authors described a regional unconformity dividing the Upper Cretaceous succession into two units characterized by different geometries. A significant difference in the structure of the Upper Cretaceous succession in the Lublin area (eastern Poland) was also noted by Hakenberg and Świdrowska [98] during their comparison of two episodes of acceleration in subsidence rate. They concluded that the reason for the first episode of high subsidence rate during Turonian is caused by the eustatic factor, whereas the period of higher rate of sediment accumulation during Early Maastrichtian is clearly related to the tectonic activity of the area.

Such a marked similarity in the structural framework of the Upper Cretaceous succession in different areas (southern, central, and eastern Poland) may indicate that a tectonic rebuilding of the sedimentary basin took place during the Late Cretaceous period.

The spatial analysis of the Upper Cretaceous succession from the area of the central part of the Carpathian Foreland is a solid reference for further detailed studies in this area.

6. Conclusions

Completed research of the Upper Cretaceous sediments of the central part of the Carpathian Foreland confirmed the complicated geological structure of the analyzed complex.

Analysis of the paleoenvironment confirmed the wide range of the elements of the depositional architecture. The alignment of these elements suggests different, time-variant directions of deposition.

At least several seismic attributes are required to visualize the various elements of the depositional architecture. Some of these elements can only be interpreted on certain attributes.

The chronostratigraphic image and Wheeler diagram allowed to identify numerous unconformities and hiatuses connected with erosive events or periods without deposition. The results of interpretation confirm earlier observations based on the cores [28]. Moreover, several dislocations were identified based on the chronostratigraphic image.

It can be unambiguously stated that the conventional structural seismic interpretation has its limitations in the view of accurate paleogeographical image recognition; only interpretation based on the chronostratigraphic image can reveal reliable results.

The interpreted Upper Cretaceous succession in the study area can be divided into two main megasequences, characterized by a diverse structure. A stratigraphic hiatus was identified between these megasequences.

The first results of detailed reconstruction of the Late Cretaceous basin paleogeography in the central part of the Carpathian Foreland and the attempt to determine the impact of both eustatic and tectonic factors on sedimentation processes were presented.

Supplementary Materials: The following are available online at <https://www.mdpi.com/article/10.3390/en14227776/s1>, Figure S1: Isopach map of the Upper Cretaceous formations in the study area; Figure S2: Detailed sequence stratigraphy and tectonostratigraphy interpretation.

Author Contributions: Conceptualization, A.U., A.L.-B. and A.K.; methodology, A.L.-B., A.K. and I.F.; software, I.F. and A.K.; validation, A.L.-B., I.F., A.K. and A.U.; formal analysis, A.U.; investigation, A.L.-B. and A.K.; writing—original draft preparation, A.U., A.K. and A.L.-B.; writing—review and editing, A.U., A.L.-B. and A.K.; visualization, A.L.-B., I.F. and A.U.; supervision: A.U., A.L.-B. and A.K. All authors have read and agreed to the published version of the manuscript.

Funding: This paper was written based on the statutory work entitled: “Seismostratigraphic analyses of the Upper Jurassic carbonate complex in the central part of the Carpathian Foreland, Part II—Upper Cretaceous Sediments”—the works of the Oil and Gas Institute–National Research Institute were commissioned by the Ministry of Science and Higher Education; order number: 44/SR/2021, archive number: DK-4100-0032/2021. The work was part of the ongoing investigation carried out by the Department of Geophysics, Faculty of Geology, Geophysics and Environmental Protection, University of Science and Technology AGH (16.16.140.315).

Institutional Review Board Statement: Not applicable.

Informed Consent Statement: Not applicable.

Data Availability Statement: Original data are not shared.

Acknowledgments: We would like to acknowledge the Polish Oil and Gas Company (PGNiG SA) for sharing the data for research purposes and to thank them for the permission to publish the results. Our gratitude goes to dGB EarthSciences and Landmark-Halliburton for granting their software to the University of Science and Technology AGH for didactic and research purposes.

Conflicts of Interest: The authors declare no conflict of interest.

References

1. Cook, T.D. Exploration History of South Texas Lower Cretaceous Carbonate Platform. *Am. Assoc. Pet. Geol. Bull.* **1979**, *63*, 32–49. [[CrossRef](#)]
2. Roehl, P.O.; Choquette, P.W. *Carbonate Petroleum Reservoirs*; Springer: Berlin/Heidelberg, Germany, 1985; pp. 32–49. [[CrossRef](#)]
3. Keeley, M.L.; Dungworth, G.; Floyd, C.S.; Forbes, G.A.; King, C.; McGarva, R.M.; Shaw, D. The Jurassic System in Northern Egypt: I. Regional Stratigraphy and Implications for Hydrocarbon Prospectivity. *J. Pet. Geol.* **1990**, *13*, 397–420. [[CrossRef](#)]
4. Alsharhan, A.S.; Magara, K. Nature and Distribution of Porosity and Permeability in Jurassic Carbonate Reservoirs of the Arabian Gulf Basin. *Facies* **1995**, *32*, 237–253. [[CrossRef](#)]
5. Gliniak, P.; Leśniak, G.; Laskowicz, R.; Such, P.; Urbaniec, A. The Facies Development and Reservoir Properties in Late Jurassic Carbonate Sediments in the Central Carpathian Foreland. In *Deformation, Fluid Flow, and Reservoir Appraisal in Foreland Fold and Thrust Belts*; Swennen, R., Roure, F., Granath, J.W., Eds.; American Association of Petroleum Geologists: Tulsa, OK, USA, 2004; Volume 1, pp. 347–355.
6. Weissenberger, J.A.W.; Wierzbicki, R.A.; Harland, N.J. Carbonate Sequence Stratigraphy and Petroleum Geology of the Jurassic Deep Panuke Field, Offshore Nova Scotia, Canada. *AAPG Mem.* **2006**, *88*, 395–431. [[CrossRef](#)]
7. Borgomano, J.; Masse, J.P.; Fenerci-Masse, M.; Fournier, F. Petrophysics of Lower Cretaceous Platform Carbonate Outcrops in Provence (SE France): Implications for Carbonate Reservoir Characterisation. *J. Pet. Geol.* **2013**, *36*, 5–41. [[CrossRef](#)]
8. Eltom, H.; Makkawi, M.; Abdullatif, O.; Alramadan, K. High-Resolution Facies and Porosity Models of the Upper Jurassic Arab-D Carbonate Reservoir Using an Outcrop Analogue, Central Saudi Arabia. *Arab. J. Geosci.* **2013**, *6*, 4323–4335. [[CrossRef](#)]
9. Morad, D.; Nader, F.H.; Gasparrini, M.; Morad, S.; Rossi, C.; Marchionda, E.; Al Darmaki, F.; Martines, M.; Hellevang, H. Comparison of the Diagenetic and Reservoir Quality Evolution between the Anticline Crest and Flank of an Upper Jurassic Carbonate Gas Reservoir, Abu Dhabi, United Arab Emirates. *Sediment. Geol.* **2018**, *367*, 96–113. [[CrossRef](#)]
10. Ahmad, S.; Wadood, B.; Khan, S.; Ahmed, S.; Ali, F.; Saboor, A. Integrating the Palynostratigraphy, Petrography, X-Ray Diffraction and Scanning Electron Microscopy Data for Evaluating Hydrocarbon Reservoir Potential of Jurassic Rocks in the Kala Chitta Range, Northwest Pakistan. *J. Pet. Explor. Prod. Technol.* **2020**, *10*, 3111–3123. [[CrossRef](#)]

11. Morycowa, E.; Moryc, W. Rozwój utworów jurajskich na Przedgórzu Karpat w rejonie Dąbrowy Tarnowskiej—Szcucina. *Rocz. Pol. Tow. Geol.* **1976**, *46*, 231–288.
12. Gutowski, J.; Urbaniec, A.; Złonkiewicz, Z.; Bobrek, L.; Świetlik, B.; Gliniak, P. Upper Jurassic and Lower Cretaceous of the Middle Polish Carpathian Foreland. *Biul. Państw. Inst. Geol.* **2007**, *426*, 1–26.
13. Świdrowska, J.; Hakenberg, M.; Poluhtovič, C.; Seghedi, A.; Višňakov, G. Evolution of the Mesozoic Basin on the Southwestern Edge of the East European Craton (Poland, Ukraine, Moldova, Romania). *Stud. Geol. Pol.* **2008**, *130*, 3–130.
14. Matyja, B.A. Development of the Mid-Polish Trough versus Late Jurassic Evolution in the Carpathian Foredeep Area. *Tethys* **2009**, *53*, 49–61.
15. Urbaniec, A.; Bobrek, L.; Świetlik, B. Litostratygrafia i charakterystyka mikropaleontologiczna utworów kredy dolnej w środkowej części przedgórza Karpat. *Prz. Geol.* **2010**, *58*, 1161–1175.
16. Krajewski, M.; Matyszkiewicz, J.; Król, K.; Olszewska, B. Facies of the Upper Jurassic-Lower Cretaceous Deposits from the Southern Part of the Carpathian Foredeep Basement in the Kraków-Rzeszów Area (Southern Poland). *Ann. Soc. Geol. Pol.* **2011**, *81*, 269–290.
17. Kosakowski, P.; Leśniak, G.; Krawiec, J. Reservoir Properties of the Palaeozoic—Mesozoic Sedimentary Cover in the Kraków—Lubaczów Area (SE Poland). *Ann. Soc. Geol. Pol.* **2012**, *82*, 51–64.
18. Urbaniec, A. Charakterystyka litofacyjna utworów jury górnej i kredy dolnej w rejonie Dąbrowa Tarnowska—Dębica w oparciu o interpretację danych sejsmicznych i otworowych. *Pr. Nauk. Inst. Nafty Gazu* **2021**, *232*, 1–240. [[CrossRef](#)]
19. Rutkowski, J. Senonian in the Area of Miechów, Southern Poland. *Rocz. Pol. Tow. Geol.* **1965**, *35*, 3–53.
20. Marcinowski, R. The Transgressive Cretaceous (Upper Albian through Turonian). *Acta Geol. Pol.* **1974**, *24*, 117–217.
21. Marcinowski, R.; Radwański, A. The Mid-Cretaceous Transgression onto the Central Polish Uplands (Marginal Part of the Central European Basin). *Zitteliana* **1983**, *10*, 65–96.
22. Kudrewicz, R.; Oleszwska-Nejbert, D. Upper Cretaceous “Echinoidlagerstätten” in the Kraków Area. *Ann. Soc. Geol. Pol.* **1997**, *67*, 1–12.
23. Remin, Z. Biostratigraphy of the Santonian in the SW Margin of the Holy Cross Mountains near Lipnik, a Potential Reference Section for Extra-Carpathian Poland. *Acta Geol. Pol.* **2004**, *54*, 587–596.
24. Jurkowska, A. Inoceramid Stratigraphy and Depositional Architecture of the Campanian and Maastrichtian of the Miechów Synclinorium (Southern Poland). *Acta Geol. Pol.* **2016**, *66*, 59–84. [[CrossRef](#)]
25. Jawor, W.; Jawor, E. Perspektywy poszukiawcze w piaskowcach cenomanu na przykładzie złoża gazu ziemnego Ryłowa. *Nafta* **1989**, *45*, 3–9.
26. Jędrzejowska-Zwinczak, H.; Jawor, E.; Żuławiński, K. Nowe elementy w interpretacji danych sejsmicznych dla utworów cenomańskich na przedgórzu Karpat. *Prz. Geol.* **1996**, *44*, 375–380.
27. Marzec, P.; Pietsch, K. Thin-Bedded Strata and Tuning Effect as Causes of Seismic Data Anomalies in the Top Part of the Cenomanian Sandstone in the Grobla-Rajsko-Ryłowa Area (Carpathian Foreland, Poland). *Geol. Q.* **2012**, *56*, 691–710. [[CrossRef](#)]
28. Heller, I.; Moryc, W. Stratygrafia utworów kredy górnej przedgórza Karpat. *Biul. Inst. Geol.* **1984**, *24*, 63–108.
29. Baran, U.; Jawor, E. Nowe możliwości poszukiawcze złóż ropy naftowej i gazu ziemnego w obszarze Jastrząbka-Żukowice-Pilzno. *Nafta* **1988**, *44*, 161–166.
30. Karnkowski, P. Uwarunkowania akumulacji węglowodorów na obszarze przedgórza Karpat. *Nafta-Gaz* **1999**, *11*, 665–678.
31. Chopra, S.; Marfurt, K.J. *Seismic Attributes for Prospect Identification and Reservoir Characterization*; Society of Exploration Geophysicists, European Association of Geoscientists and Engineers: Tulsa, OK, USA, 2005.
32. Chopra, S.; Marfurt, K.J. Seismic attribute expression of differential compaction. *Leading Edge* **2012**, *31*, 1418–1422. [[CrossRef](#)]
33. Torrado, L.; Mann, P.; Bhattacharya, J. Application of seismic attributes and spectral decomposition for reservoir characterization of a complex fluvial system: Case study of the Carbonera Formation, Llanos foreland basin, Colombia. *Geophysics* **2014**, *79*, B221–B230. [[CrossRef](#)]
34. Li, X.; Chen, Q.; Wu, C.; Liu, H.; Fang, Y. Application of multi-seismic attributes analysis in the study of distributary channels. *Mar. Pet. Geol.* **2016**, *75*, 192–202. [[CrossRef](#)]
35. El Redini, N.A.H.; Bakr, A.M.A.; Dahroug, S.M. Seismic data interpretation for hydrocarbon potential, for Safwa/Sabbar field, East Ghazalat onshore area, Abu Gharadig basin, Western Desert, Egypt. *NRIAG J. Astron. Geophys.* **2017**, *6*, 287–299. [[CrossRef](#)]
36. Anees, A.; Shi, W.; Ashraf, U.; Xu, Q. Channel identification using 3D seismic attributes in lower Shihezi Formation of Hangjinqi area, northern Ordos Basin, China. *J. Appl. Geophys.* **2019**, *163*, 139–150. [[CrossRef](#)]
37. Karnkowski, P.; Głowacki, E. O budowie geologicznej utworów podmiocennych przedgórza Karpat Środkowych. *Kwart. Geol.* **1961**, *5*, 372–419.
38. Obuchowicz, Z. Budowa geologiczna przedgórza Karpat środkowych. *Pr. Inst. Geol.* **1963**, *30*, 321–354.
39. Stemulak, J.; Jawor, E. Wgłębna budowa geologiczna przedgórza Karpat w obszarze na zachód od Dunajca i Wisły. *Kwart. Geol.* **1963**, *7*, 169–186.
40. Jawor, E. Wgłębna budowa geologiczna na wschód od Krakowa. *Acta Geol. Pol.* **1970**, *20*, 709–770.
41. Machaniec, E.; Zapałowicz-Bilan, B. Foraminiferal Biostratigraphy and Paleobathymetry of Senonian Marls (Upper Cretaceous) in the Vicinity of Kraków (Januszowice-Korzkiew Area, Bonarka Quarry). *Stud. Geol. Pol.* **2005**, *124*, 285–295.
42. Moryc, W. Budowa geologiczna podłoża miocenu w rejonie Kraków-Pilzno. Część 2. Perm i mezozoik. *Nafta-Gaz* **2006**, *6*, 263–282.

43. Walaszczyk, I.; Cieśliński, S.; Sylwestrzak, H. Selected Geosites of Cretaceous Deposits in Central and Eastern Poland. *Pol. Geol. Inst. Spec. Pap.* **1999**, *2*, 71–76.
44. Moryc, W.; Jachowicz, M. Utwory prekambryjskie w rejonie Bochnia-Tarnów-Dębica. *Prz. Geol.* **2000**, *48*, 601–606.
45. Jachowicz-Zdanowska, M. Organic Microfossil Assemblages from the Late Ediacaran Rocks of the Małopolska Block, Southeastern Poland. *Geol. Q.* **2011**, *55*, 85–94.
46. Zając, R. Stratygrafia i rozwój facjalny dewonu i dolnego karbonu południowej części podłoża zapadliska przedkarpackiego. *Kwart. Geol.* **1984**, *28*, 291–316.
47. Moryc, W. Budowa geologiczna podłoża miocenu w rejonie Kraków-Pilzno. Część 1. Prekambr i paleozoik (bez permu). *Nafta-Gaz* **2006**, *5*, 197–216.
48. Urbaniec, A.; Bartoń, R.; Bajewski, Ł.; Wilk, A. Wyniki interpretacji strukturalnej utworów triasu i paleozoiku przedgórze Karpat opartej na nowych danych sejsmicznych. *Nafta-Gaz* **2020**, *9*, 559–568. [[CrossRef](#)]
49. Jasionowski, M. Zarys litostratygrafii osadów miocenijskich wschodniej części zapadliska przedkarpackiego. *Biul. Państw. Inst. Geol.* **1997**, *375*, 43–59.
50. Urbaniec, A.; Stadtmüller, M.; Bartoń, R. Possibility of a More Detailed Seismic Interpretation within the Miocene Formations of the Carpathian Foredeep Based on the Well Logs Interpretation. *Nafta-Gaz* **2019**, *9*, 527–544. [[CrossRef](#)]
51. Hakenberg, M.; Świdrowska, J. Evolution of the Holy Cross Segment of the Mid-Polish Trough during the Cretaceous. *Kwart. Geol.* **1998**, *42*, 239–261.
52. Peryt, D.; Wyrwicka, K. “Zdarzenie beztlenowe” na granicy cenomanu i turonu w Polsce południowo-wschodniej. *Prz. Geol.* **1989**, *37*, 563–569.
53. Leary, P.N.; Peryt, D. The Late Cenomanian Oceanic Anoxic Event in the Western Anglo-Paris Basin and Southeast Danish-Polish Trough: Survival Strategies of and Recolonisation by Benthonic Foraminifera. *Hist. Biol.* **1991**, *5*, 321–338. [[CrossRef](#)]
54. de Bruin, G.; McBeath, K.; Hemstra, N. Unravelling a Carbonate System: Technical Advances in Seismic Sequence Stratigraphy. *First Break* **2007**, *25*, 57–61. [[CrossRef](#)]
55. de Groot, P.; Huck, A.; De Bruin, G.; Hemstra, N.; Bedford, J. The Horizon Cube: A Step Change in Seismic Interpretation! *Lead. Edge* **2010**, *9*, 1048–1055. [[CrossRef](#)]
56. Ligtenberg, H.J.; de Bruin, G.; Hemstra, N.; Geel, C. Sequence Stratigraphic Interpretation in the Wheeler Transformed (Flattened) Seismic Domain. In Proceedings of the 68th European Association of Geoscientists and Engineers Conference and Exhibition Incorporating SPE EUROPEC 2006: Opportunities in Mature Areas, Vienna, Austria, 12–15 June 2006.
57. Qayyum, F.; de Groot, P.; Hemstra, N. Using 3D Wheeler Diagrams in Seismic Interpretation—The Horizon Cube Method. *First Break* **2012**, *30*, 103–109. [[CrossRef](#)]
58. Watkinson, M.P.; Hart, M.B.; Joschi, A. Cretaceous Tectonostratigraphy and the Development of the Cauvery Basin, Southeast India. *Pet. Geosci.* **2007**, *13*, 181–191. [[CrossRef](#)]
59. Haqiqie, F.A.; Sunardi, E.; Ilmii, N.N.; Ginting, A.S. Determination of Potential Hydrocarbon and Tectonostratigraphy Analysis Based on 2D Seismic in Padamarang Sub-Basin, Bone Basin, South Part of Sulawesi. *J. Geol. Sci. Appl. Geol.* **2018**, *2*, 38–48.
60. Nikishin, A.M.; Kopaeovich, L.F. Tectonostratigraphy as a Basis for Paleotectonic Reconstructions. *Moscow Univ. Geol. Bull.* **2009**, *64*, 65–74. [[CrossRef](#)]
61. Qayyum, F.; Catuneanu, O.; de Groot, P. Historical Developments in Wheeler Diagrams and Future Directions. *Basin Res.* **2015**, *27*, 336–350. [[CrossRef](#)]
62. McDonough, K.J.; Bouanga, E.; Pierard, C.; Horn, B.; Emmet, P.; Gross, J.; Danforth, A.; Sterne, N.; Granath, J. Wheeler-Transformed 2D Seismic Data Yield Fan Chronostratigraphy of Offshore Tanzania. *Lead. Edge* **2013**, *32*, 162–170. [[CrossRef](#)]
63. Ramirez, F.A. Tectonostratigraphic Evolution of a Suprasalt Minibasin, Oligocene-Miocene Western Slope of the Gulf of Mexico. Master’s Thesis, University of Texas, El Paso, TX, USA, 2016.
64. Mantilla, O.; Castellanos, J.; Ramirez, V.; Hurtado, D.; Rubio, C. Tectono-stratigraphic Events of the Northern Caribbean Offshore Colombia. In Proceedings of the AAPG International Conference and Exhibition, Cartagena, Colombia, 8–11 September 2013.
65. Kenyon, I.C.; McClay, K.; Scarselli, N. 4-D Tectono-Stratigraphy, Inverted Fault Architecture and Implications on Hydrocarbon Migration within the Taranaki Basin, Offshore New Zealand.pdf. 2016. Available online: https://figshare.com/articles/journal_contribution/4-D_Tectono-stratigraphy_Inverted_Fault_Architecture_and_implications_on_Hydrocarbon_Migration_within_the_Taranaki_Basin_Offshore_New_Zealand_pdf/4253771/1 (accessed on 1 November 2021).
66. Koson, S.; Chenrai, P.; Choowong, M. Seismic Attributes and Their Applications in Seismic Geomorphology. *Bull. Earth Sci. Thail.* **2014**, *6*, 1–9.
67. Sarhan, M.A. The efficiency of seismic attributes to differentiate between massive and non-massive carbonate successions for hydrocarbon exploration activity. *NRIAG J. Astron. Geophys.* **2017**, *6*, 311–325. [[CrossRef](#)]
68. Bartoń, R.; Urbaniec, A. Wykorzystanie pomiarów PPS do uszczegółowienia interpretacji sejsmicznej 3D na przykładzie utworów dolnego paleozoiku. *Nafta-Gaz* **2018**, *9*, 655–668. [[CrossRef](#)]
69. Ashraf, U.; Zhu, P.; Yasin, Q.; Anees, A.; Imraz, M.; Mangi, H.N.; Shakeel, S. Classification of reservoir facies using well log and 3D seismic attributes for prospect evaluation and field development: A case study of Sawan gas field, Pakistan. *J. Pet. Sci. Eng.* **2019**, *175*, 338–351. [[CrossRef](#)]
70. Taner, M.T.; Koehler, F.; Sheriff, R.E. Complex Seismic Trace Analysis. *Geophysics* **1979**, *44*, 1041–1063. [[CrossRef](#)]

71. Ulrych, T.; Sacchi, M.; Graul, M.; Taner, M.T. Instantaneous Attributes: The What and the How. *Explor. Geophys.* **2007**, *38*, 213–219. [[CrossRef](#)]
72. Fashagba, I.; Erikanselu, P.; Lanisa, A.; Matthew, O. Seismic Reflection Pattern and Attribute Analysis as a Tool for Defining Reservoir Architecture in ‘SABALO’ Field, Deepwater Niger Delta. *J. Pet. Explor. Prod. Technol.* **2020**, *10*, 991–1008. [[CrossRef](#)]
73. Hart, B.S. Channel Detection in 3-D Seismic Data Using Sweetness. *Am. Assoc. Pet. Geol. Bull.* **2008**, *92*, 733–742. [[CrossRef](#)]
74. Zheng, J.; Peng, G.; Sun, J.; He, D.; Qin, D. Fluid Detection of Sand-Shale Interbeds Based on a “New Sweetness” Attribute. In Proceedings of the 2017 SEG International Exposition and 88th Annual Meeting, Houston, TX, USA, 24–29 September 2017; pp. 3428–3432.
75. Łaba-Biel, A.; Kwietniak, A.; Urbaniec, A. Seismic Identification of Unconventional Heterogenous Reservoirs Based on Depositional History—A Case Study of the Polish Carpathian Foredeep. *Energies* **2020**, *13*, 6036. [[CrossRef](#)]
76. Partyka, G.A. Seismic Thickness Estimation: Three Approaches, Pros and Cons. In Proceedings of the 2001 SEG Annual Meeting, San Antonio, TX, USA, 9–14 September 2001.
77. Puryear, C.I.; Castagna, J.P. Layer-Thickness Determination and Stratigraphic Interpretation Using Spectral Inversion: Theory and Application. *Geophysics* **2008**, *73*, R37–R48. [[CrossRef](#)]
78. Partyka, G.; Gridley, J.; Lopez, J. Interpretational Applications of Spectral Decomposition in Reservoir Characterization. *Lead. Edge* **1999**, *18*, 353–360. [[CrossRef](#)]
79. Wang, X.; Zhang, B.; Li, F.; Qi, J.; Bai, B. Seismic Time-Frequency Decomposition by Using a Hybrid Basis-Matching Pursuit Technique. *Interpretation* **2016**, *4*, T239–T248. [[CrossRef](#)]
80. Tary, J.B.; Herrera, R.H.; Han, J.; van der Baan, M. Spectral Estimation—What Is New? What Is Next? *Rev. Geophys.* **2014**, *52*, 723–749. [[CrossRef](#)]
81. Porebski, S.J.; Warchoń, M. Hyperpycnal Flows and Deltaic Clinofolds—Implications for Sedimentological Interpretations of Late Middle Miocene Fill in the Carpathian Foredeep Basin. *Prz. Geol.* **2006**, *54*, 421–429.
82. Pietsch, K.; Porebski, S.J.; Marzec, P. The Use of Seismostratigraphy for Exploration of Miocene Gas-Bearing Reservoir Facies in the NE Part of the Carpathian Foreland Basin (Poland). *Geologia* **2010**, *36*, 173–186.
83. Kwietniak, A.; Cichostępski, K.; Kasperska, M. Spectral Decomposition Using the CEEMD Method: A Case Study from the Carpathian Foredeep. *Acta Geophys.* **2016**, *64*, 1525–1541. [[CrossRef](#)]
84. Posamentier, H.W.; Kolla, V. Seismic Geomorphology and Stratigraphy of Depositional Elements in Deepwater Settings. *J. Sediment. Res.* **2003**, *73*, 367–388. [[CrossRef](#)]
85. Catuneanu, O. *Principles of Sequence Similarity*; Elsevier: Edmonton, AL, Canada, 2006.
86. Catuneanu, O.; Abreu, V.; Bhattacharya, J.P.; Blum, M.D.; Dalrymple, R.W.; Eriksson, P.G.; Fielding, C.R.; Fisher, W.L.; Galloway, W.E.; Gibling, M.R.; et al. Towards the Standardization of Sequence Stratigraphy. *Earth-Sci. Rev.* **2009**, *92*, 1–33. [[CrossRef](#)]
87. Catuneanu, O.; Galloway, W.E.; Kendall, C.G.S.C.; Miall, A.D.; Posamentier, H.W.; Strasser, A.; Tucker, M.E. Sequence Stratigraphy: Methodology and Nomenclature. *Newsl. Stratigr.* **2011**, *44*, 173–245. [[CrossRef](#)]
88. Loucks, R.G.; Sarg, J.F. *Carbonate Sequence Stratigraphy—Recent Developments and Applications*; The American Association of Petroleum Geologists: Tulsa, OK, USA, 1993; Volume 57.
89. Zecchin, M.; Catuneanu, O. High-Resolution Sequence Stratigraphy of Clastic Shelves VI: Mixed Siliciclastic-Carbonate Systems. *Mar. Pet. Geol.* **2017**, *88*, 712–723. [[CrossRef](#)]
90. Cumberpatch, Z.A.; Soutter, E.L.; Kane, I.A.; Casson, M.; Vincent, S.J. Evolution of a Mixed Siliciclastic-Carbonate Deep-Marine System on an Unstable Margin: The Cretaceous of the Eastern Greater Caucasus, Azerbaijan. *Basin Res.* **2021**, *33*, 612–647. [[CrossRef](#)]
91. Embry, A.F. Sequence Boundaries and Sequence Hierarchies: Problems and Proposals. *Stratigr. Northwest Eur. Margin Spec. Publ.* **1995**, *5*, 1–11.
92. Donaldson, W.S.; Plint, A.G.; Longstaffe, F.J. Tectonic and Eustatic Control on Deposition and Preservation of Upper Cretaceous Ooidal Ironstone and Associated Facies: Peace River Arch Area, NW Alberta, Canada. *Sedimentology* **1999**, *46*, 1159–1182. [[CrossRef](#)]
93. Porebski, S.J. Podstawy stratygrafii sekwencji w sukcesjach klastycznych. *Prz. Geol.* **1996**, *44*, 995–1006.
94. Phillips, T.B.; Jackson, C.A.L.; Norcliffe, J.R. Pre-Inversion Normal Fault Geometry Controls Inversion Style and Magnitude, Farsund Basin, Offshore Southern Norway. *Solid Earth* **2020**, *11*, 1489–1510. [[CrossRef](#)]
95. King, P.R.; Thrasher, G.P. *Cretaceous-Cenozoic Geology and Petroleum Systems of the Taranaki Basin, New Zealand*; Institute of Geological and Nuclear Sciences Monograph 13. Institute of Geological and Nuclear Sciences: Lower Hutt, New Zealand, 1996.
96. Martin-Chivelet, J. Sequence Stratigraphy of Mixed Carbonate-siliciclastic Platforms Developed in a Tectonically Active Setting, Upper Cretaceous, Betic Continental Margin (Spain). *J. Sediment. Res.* **1995**, *B65*, 235–254. [[CrossRef](#)]
97. Mortimore, R.; Pomerol, B. Upper Cretaceous tectonic phases and end Cretaceous inversion in the Chalk of the Anglo-Paris Basin. *Proc. Geol. Assoc.* **1997**, *108*, 231–255. [[CrossRef](#)]
98. Hakenberg, M.; Świdrowska, J. Cretaceous basin evolution in the Lublin area along the Teisseyre-Tornquist zone (SE Poland). *Ann. Soc. Geol. Pol.* **2001**, *71*, 1–20.
99. Krzywiec, P.; Gutowski, J.; Walaszczyk, I.; Wróbel, G.; Wybraniec, S. Tectonostratigraphic model of the Late Cretaceous inversion along the Nowe Miasto–Zawichost Fault Zone, SE Mid-Polish Trough. *Geol. Q.* **2009**, *53*, 27–48.

100. Krzywiec, P.; Stachowska, A. Late Cretaceous Inversion of the NW Segment of the Mid-Polish Trough—How Marginal Troughs Were Formed, and Does It Matter at All? *Ger. J. Geol.* **2016**, *167*, 107–119. [[CrossRef](#)]
101. Ahlrichs, N.; Noack, V.; Hübscher, C.; Seidel, E.; Warwel, A.; Kley, J. Impact of Late Cretaceous inversion and Cenozoic extension on salt structure growth in the Baltic sector of the North German Basin. *Basin Res.* **2021**, *33*, 1–31. [[CrossRef](#)]
102. Stachowska, A.; Krzywiec, P. Depositional Architecture of the Upper Cretaceous Succession in Central Poland (Grudziądz-Polik Area) Based on Regional Seismic Data. *Geol. Q.* **2021**, *65*, 1–17. [[CrossRef](#)]
103. Voigt, T.; Kley, J.; Voigt, S. Dawn and Dusk of Late Cretaceous Basin Inversion in Central Europe. *Solid Earth* **2021**, *12*, 1443–1471. [[CrossRef](#)]
104. Xiao, H.B.; Suppe, J. Origin of Rollover. *Am. Assoc. Pet. Geol. Bull.* **1992**, *76*, 509–529.
105. Gui, B.; He, D.; Chen, W.; Zhang, W. Migration of Growth Axial Surfaces and Its Implications for Multiphase Tectono-Sedimentary Evolution of the Zhangwu Fault Depression, Southern Songliao Basin, NE China. *J. Geodyn.* **2014**, *75*, 53–63. [[CrossRef](#)]
106. Szász, L.; Ion, J. Crétacé Supérieur Du Bassin de Babadag. *Mémoires Inst. Géologie Géophysique* **1988**, *33*, 91–149.
107. Walaszczyk, I. Turonian through Santonian Deposits of the Central Polish Uplands; Their Facies Development, Inoceramid Paleontology and Stratigraphy. *Acta Geol. Pol.* **1992**, *42*, 1–122.
108. Leszczyński, K. The Upper Cretaceous Carbonate-Dominated Sequences of the Polish Lowlands. *Geol. Q.* **1997**, *41*, 521–531.
109. Świdrowska, J.; Hakenberg, M. Subsidence and Problem of Incipient in the Mid-Polish Trough Based on Thickness Maps and Cretaceous Lithofacies Analysis. *Prz. Geol.* **1999**, *48*, 61–68.
110. Krzywiec, P. Structural Inversion of the Pomeranian and Kuiavian Segments of the Mid-Polish Trough—Lateral Variations in Timing and Structural Style. *Geol. Q.* **2006**, *50*, 151–168.
111. Jasionowski, M. A Cretaceous Non-depositional Surface in the Kraków Upland (Mydlniki, Zabierzów): Burrows, Borings and Stromatolites. *Ann. Soc. Geol. Pol.* **1995**, *65*, 63–77.